SUPPORTING INFORMATION

Subwavelength lattice optics by evolutionary design

Mark D. Huntington,[1] Lincoln J. Lauhon,[1] and Teri W. Odom[1,2,*]

[1]Department of Materials Science and Engineering, Northwestern University, Evanston, Illinois 60208, USA

[2]Department of Chemistry, Northwestern University, Evanston, Illinois 60208, USA

*e-mail: todom@northwestern.edu

Description of the Lattice Evolution Algorithm

We developed our lattice evolution algorithm (LEA) as a type of evolutionary algorithm (EA) that uses ideas from Darwin's "survival of the fittest" to find the optimal solution to a problem.[1-3] Typically for EAs, all of the variables that describe the system being optimized need to be cast onto "DNA," which is typically a large binary array. In our LEA, each position in the lattice is represented by a location in the DNA string. In this work, we explore focusing from a square patch that is 10 μm × 10 μm with a square nanohole array (a_0 = 300 nm, d = 150 nm); therefore there are 1089 positions in the DNA array. For a single phase elements, a hole is represented as a "1" and no-hole is a "0." For example, if there was a hole in the center of the lattice (row: 17, column: 17) there would be a 1 in the 578th position in the DNA string. **Figure S1** shows a binary representation of a lattice with a random arrangement of nanoholes.

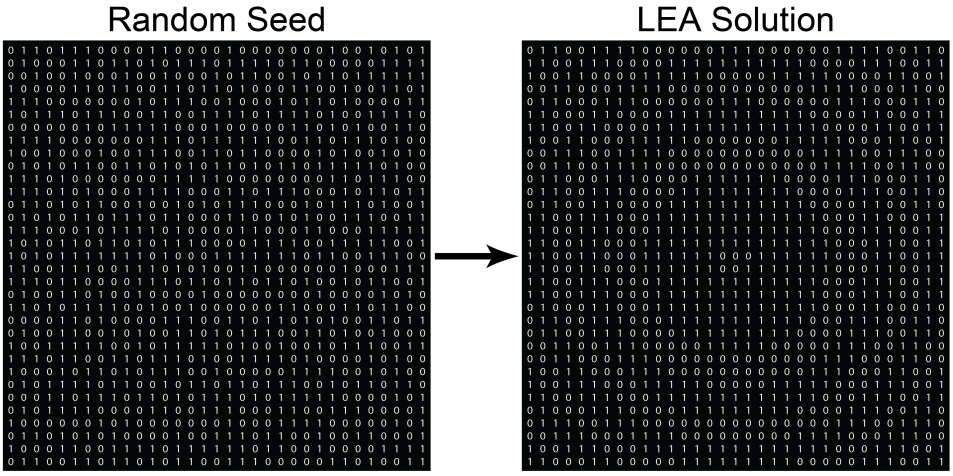

Figure S1: Binary representation of a lattice opto-materials at the beginning (left) and end (right) of the LEA.

Our LEA tracks the evolution of a "population" where each individual in the population has its own DNA and represents a solution to the design problem. The population size is a design parameter and was determined to be 600 during the

optimization of the algorithm. To start, each member in the population was given a randomly generated DNA, which represents a specific nanohole configuration. **Code section 1** shows how the initial population was seeded in the LEA.

Code section 1: Set up initial random population.

```
for ii ← 1 to Population Size do
    for jj ← 1 to DNA Length do
        generate a random number between 0 and 1;
        if the random number is greater than 0.5 then
            for population member ii, set DNA array value at jj to 1
            ("open");
        else
            for population member ii, set DNA array value at jj to 0
            ("closed");
        end
    end
end
```

All random numbers in the algorithm were generated using a Mersenne Twister pseudo random number generator that was seeded with the Unix system time as a seed. The start times of all simulations were offset by a random time to further ensure that all simulations had independent random numbers.

The far field profiles were then calculated for each of the members of the initial population using the point source method (**Fig. S2**) for lattices with a single phase element or finite difference time domain (FDTD) simulations for lattices with multiple phase units (**Fig. S4**). The details of calculating field profiles from the point source approximation are given in a later section p. S9. To increase the speed of the LEA, we used a separate program to calculate the real and imaginary parts of the electric field (E_x, E_y and E_z) and stored them in data files. Then, at the beginning of the LEA, we loaded the field points in a 2 μm × 2 μm *x*-*z* plane containing the desired focal point (**Fig. S3**), which resulted in 400 field points on a 50-nm grid, into an array. **Code section 2** shows how the field points were loaded at the beginning of the simulation. These fields represent the 3D projection of electric fields from all 1089 nanoholes in a gold film.

Code section 2: Load complex field data in a window around the focal point.

```
for ii ← 1 to number of holes in x (33) do
    for jj ← 1 to number of holes in y (33) do
        Load data file for hole at index ii and jj containing complex fields
        (E_x, E_y and E_z);
        for kk ← 1 to number of x-Pixels (20) do
            for ll ← 1 to number of z-Pixels (20) do
                Put field data (E_x, E_y and E_z) into large array at the
                DNA index (ii * (number of holes in y) + jj) and spatial
                location indices (kk, ll);
            end
        end
    end
end
```

During the simulation, to calculate the electric field profile for a specific nanohole configuration, only fields that corresponded to "open" holes were added in the complex plane (**code section 3**).

Code section 3: Calculate electric field intensity.

```
for ii ← 1 to population size do
    for jj ← 1 to number of x-Pixels (20) do
        for kk ← 1 to number of z-Pixels (20) do
            Set the array for the sum of fields to zero;
        end
    end
    for jj ← 1 to DNA Length do
        if the hole at the DNA index (jj) is "open" then
            for kk ← 1 to number of x-Pixels (20) do
                for ll ← 1 to number of z-Pixels (20) do
                    Add the complex fields for the hole at DNA index (jj)
                    to the sum of fields;
                end
            end
        end
    end
end
```

Next, the fitness of each member of the population was calculated by evaluating the fitness function. In order to evaluate the fitness, we first needed to calculate the electric field intensity

for all of the members of the population (**code section 4**). The fitness function to focus light at a specific location was given in equation 1. We used a small constant *c* to ensure that the fitness function did not go to infinity when the maximum intensity was at the desired focal point. Both *d* and *I* can be computed in the same loop as the field intensity (**code section 4**).

Code section 4: Calculation of the fitness.

```
for ii ← 1 to population size do
    For population member ii set the maximum value and distance to
    zero;
    for jj ← 1 to number of x-Pixels (20) do
        for kk ← 1 to number of z-Pixels (20) do
            if Intensity at pixel (jj, kk) is greater than maximum value for
            population memberii then
                Set the maximum value for population member ii to the
                intensity at pixel (jj, kk);
                Set the distance population member ii to the distance of
                pixel (jj, kk);
            end
        end
    end
    Calculate the fitness for population member ii from the maximum
    value and distance;
end
```

After the fitness was evaluated for all of the members of the population was sorted by fitness using a bubble sort algorithm (**code section 5**). Importantly, after the first generation of the algorithm, 50% of the solutions from the previous generation were sorted along with the current generation. The index that represents the location of the DNA array for a specific nanohole configuration was sorted and stored along with the fitness.

Code section 5: Sort population based on the fitness.

```
for ii ← 1 to 2 × population size do
    for jj ← 1 to population index ii do
        if Fitness of population member ii is greater than the fitness of
        population member jj then
            Swap position of population members ii and jj;
        end
    end
end
```

Combining pairs of the initial population then created a new generation of the population. The pairs were selected by using a modified roulette wheel selection method so that the members with a higher fitness function were selected. **Code section 6** shows the roulette wheel selection method. In brief, a random number was generated between zero and the maximum fitness value, then a random member of the population was selected, if that member's fitness was greater than the random number then the member is selected as one of the contributing pairs, if not the

Code section 6: Select members to be "parents" for the next generation.

```
for ii ← 1 to 7/8^ths of the population size do
    while number of parents found is less than 2 do
        Select a random member of the population;
        if Fitness of randomly selected member is greater than a random
        number × the maximum fitness then
            Save parent index;
            Increase the number of parents found by 1;
        end
    end
end
```

process is repeated. Since the fitness of previous generations was included in the sorting step above, for all generations after the first generation the top 50% of the population from the previous generation was also eligible for selection during the combination process.

Once two members of the initial population were selected, their DNA was combined by breaking the DNA string into small sections called chromosomes. In our LEA, each chromosome contained 3 binary numbers. To combine the DNA chromosomes were selected randomly from either of the initial two solutions. For example, the first 9 bits of the DNA string for one of the members of the new population could be composed of two chromosomes from one of the members of the pair (DNA_1) and the third chromosome from the other member (DNA_2). Therefore, the first 9 bits of the new DNA string would be: $DNA_{new}(1\text{-}9) = [DNA_1(1), DNA_1(2), DNA_1(3), DNA_1(4), DNA_1(5), DNA_1(6), DNA_2(7), DNA_2(8), DNA_2(9)]$. **Code section 7** shows the implementation of the combination process.

In addition to the combination of DNA, we included a mutation process where either of the binary numbers in the DNA string can randomly switch to the opposite number. The probability of a number switching is given by the mutation rate. After optimizing the LEA, we chose a mutation rate of 0.001. Since the length of the DNA string was 1089, a mutation rate of 0.001 means that on average, one bit in the DNA string will be randomly flipped during mutation. The code that executes the mutation process is integrated with the DNA combination and is shown in **code section 7**.

Code section 7: Combine DNA of parents and perform mutation.

```
while DNA index is less than DNA length do
    generate a random number between 0 and 1;
    if the random number is greater than 0.5 then
        for ii ← 1 to chromosome length (3) do
            Take value DNA array for parent 1;
            generate a random number between 0 and 1;
            if the random number is less than the mutation rate (0.001)
            then
                Change the value DNA array to the opposite value;
            end
        end
    else
        for ii ← 1 to chromosome length (3) do
            Take value DNA array for parent 2;
            generate a random number between 0 and 1;
            if the random number is less than the mutation rate (0.001)
            then
                Change the value DNA array to the opposite value;
            end
        end
    end
end
```

The members of the new population made by combining pairs from the previous generation and mutating make up 7/8 of the new population. To increase the diversity of our population, we filled 1/8 of the new population with randomly generated DNA. The DNA for these members was generated in the same way as the initial population (code section 1).

At the end of every generation, the bottom 50% of the population was removed and the arrays were rearranged to make room for the new generation. This cycle continued until the LEA converged on the optimal solution by reaching a convergence condition, which we defined when the fittest member in the population did not change for 30 generations.

Point-source Simulation Method

To simulate the far-field optical profiles and to analyze the fitness functions (*F*), we carried out analytical calculations by considering each nanohole in the lattice opto-material as a point source of light.[4] In this approximation, the material properties of the gold film are not considered. The electric field intensity was computed by adding the complex components in the far-field, which considers the distance from the point source, wavelength, and the refractive index environment. A detailed description of the point-source method (**Fig. S2**) and derivation (Equations S1-S9) is given below.

To calculate the far-field profile of the lattice opto-materials, we considered each of the nanoholes in the lattice opto-material as a single point source.[4] Then, each of the six components ($Re(E_x)$), ($Im(E_x)$), $Re(E_y)$), ($Im(E_y)$), $Re(E_z)$), and ($Im(E_z)$) of the complex field from a single hole

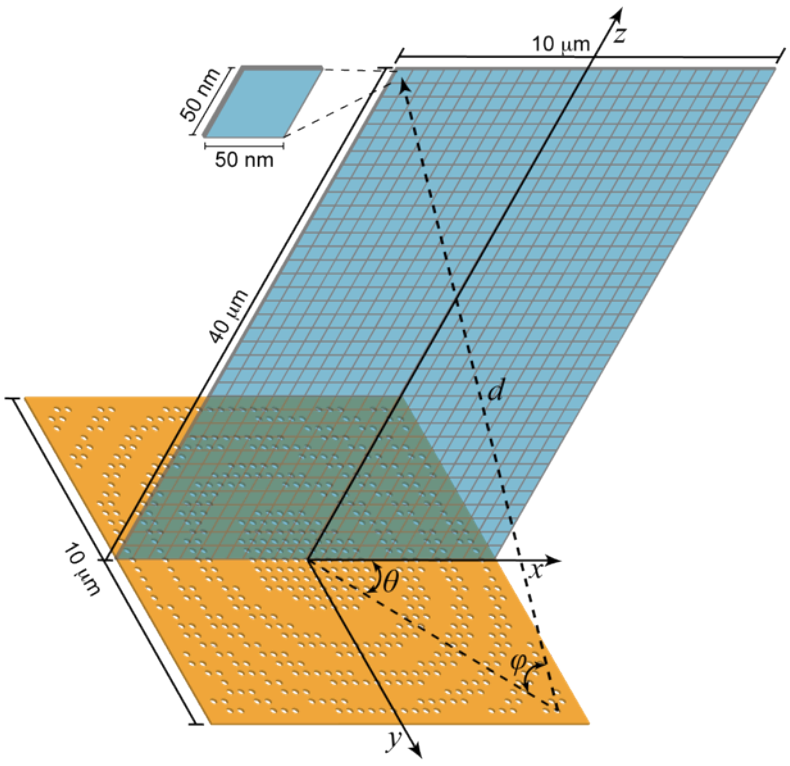

Figure S2: Scheme of point source simulation. The complex field contribution from each nanohole is calculated for each pixel in the *x*-*z* plane of the optical far field.

was saved in a file for later use by the LEA. **Figure S2** shows a scheme of how the field was calculated for each of the holes in the lattice opto-materials. For the point source approximation, we assumed that the field intensity decreased as the reciprocal of the distance from the source (*d*). Using the distance, we could calculate the electromagnetic fields for the transverse electric (TE) and transverse magnetic (TM) as

$$E_{TE} = \frac{cos(\theta)}{d} \tag{S1}$$

$$E_{TM} = \frac{sin(\theta)}{d} \tag{S2}$$

where θ is the angle between the location of the hole and the x-axis. From the two polarization components of the electric fields we could calculate the magnitude of the electric field in the x, y and z directions

$$||E_x|| = E_{TE}sin(\phi)cos(\theta) + E_{TM}sin(\theta) \tag{S3}$$

$$||E_y|| = E_{TE}sin(\phi)sin(\theta) - E_{TM}cos(\theta) \tag{S4}$$

$$||E_z|| = -E_{TE}cos(\phi) \tag{S5}$$

where ϕ is the angle between the vector *d* and the *x*-*y* plane. To calculate the complex electric field, we needed to first calculate the phase (Θ) of the light

$$\Theta = \frac{d}{n\lambda}2\pi \tag{S6}$$

where *n* is the refractive index, and λ is the wavelength of light incident on the lattice opto-material. Once the phase was calculated, the complex electric field was given by

$$E_x = ||E_x||cos(\Theta) + i||E_x||sin(\Theta) \tag{S7}$$

$$E_y = ||E_y||cos(\Theta) + i||E_y||sin(\Theta) \tag{S8}$$

$$E_z = ||E_z||cos(\Theta) + i||E_z||sin(\Theta) \tag{S9}$$

where *i* is the imaginary number. We stored both the real and imaginary parts for each of the components of the field for each nanohole position in a separate file. Thus, before starting the algorithm we had 6 × 33 × 33 (6534) files each of which contained the field points for the *x*-*z* plane (10 μm × 40 μm). The field-point size was 50 nm × 50 nm so that each file consisted of 200 × 800 (160,000) individual points.

At the beginning of the algorithm, we loaded a subset of field points corresponding to a 2 × 2 μm (40 × 40 points) window around the focal point, shown in green (**Fig. S3**) into a memory array. To calculate the field intensity in the optical far field, all of the components of the

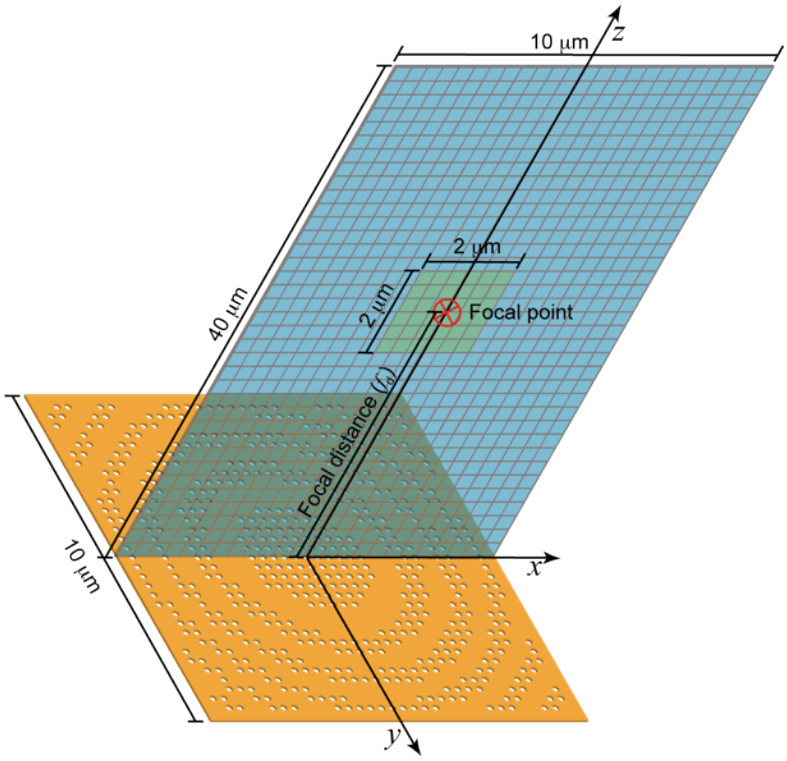

Figure S3: Schematic calculation window for the LEA. The window where the field is calculated for the LEA was centered around the focal point.

complex fields for each of the contributing holes were added within this small window. The absolute value of the field components was then calculated within this window.

Finite Difference Time Domain Simulation Method

To calculate the far-field profile of the lattices opto-materials with multiple phase elements, we calculated the far-field profile of nanoholes of different sizes using finite difference time domain (FDTD) simulations. Then, we exported each of the six components ($Re(E_x)$, $Im(E_x)$, $Re(E_y)$, $Im(E_y)$, $Re(E_z)$, and $Im(E_z)$) of the complex field from a single hole and saved them in a file for later use by the LEA. After the initial simulation, the fields were

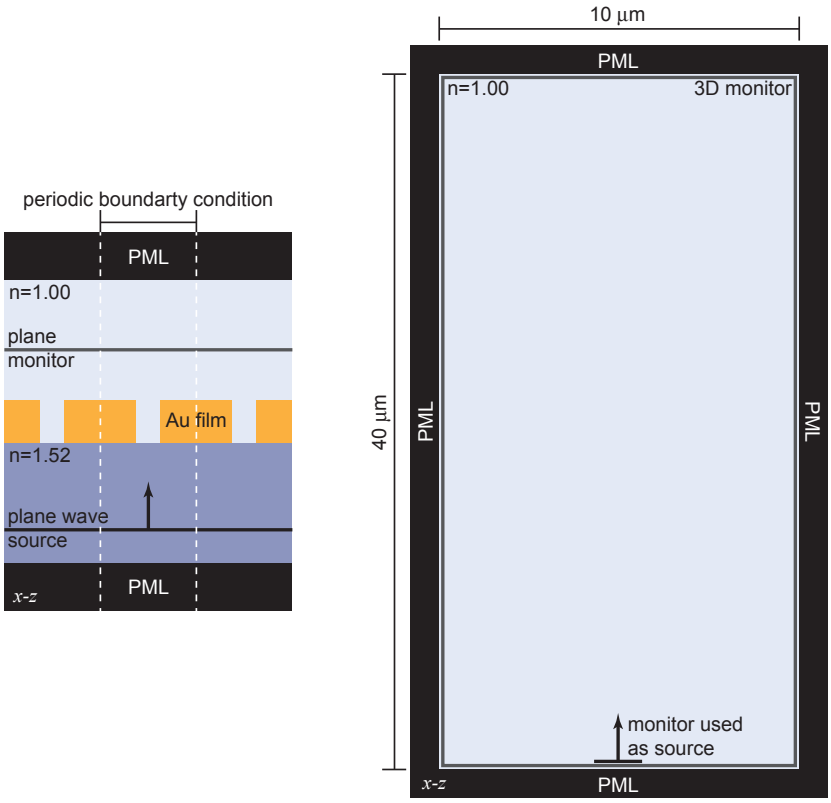

Figure S4: Scheme of FDTD simulation. Near field simulation of the transmission through a single nanohole (left) and large volume simulation of how the fields from the nanohole propagate in the far field (right).

stored in the same way as the point-source simulation method. Therefore, the LEA did not have to change. **Figure S4** shows a scheme of how the field was calculated for each of the holes in the lattice opto-material. For FDTD, we separated the simulation into two parts to reduce the overall

simulation time. The first FDTD simulation calculated the transmission from a single nanohole within an array of nanoholes in a Au film (**Fig. S4**, left). Because of the imaginary part of the dielectric constant for Au, we used a 4-nm mesh for this simulation. We then took the fields that were recorded at the monitor in the first simulation and projected them over a large volume in a second FDTD simulation (**Fig. S4**, right). Since the entire volume in the second simulation is filled with a simple dielectric we could use a much larger 50-nm mesh size for this calculation.

Lattice Evolution Algorithm Performance

For a 10 μm × 10 μm square array (lattice constant, a_0 = 300 nm), there are 33 × 33 elements, which results in 2^{1089} or ~10^{300} total possible arrangements of holes. The largest number of configurations that could be calculated in a year on a supercomputer is ~2^{70}. Assuming that computer speeds continue to increase according to Moore's law, a computer that could calculate all possible solution will not be developed for ~1200 years. Using our LEA with optimal parameters, we could design a lattice opto-material in ~210 generations solving for only ~2x10^5 structures. Thus, the LEA could be computed in ~ 0.45 cpu hours (27 minutes). **Figure S5** shows that after ~100 – 150 generations the LEA fitness for all focal distances is within

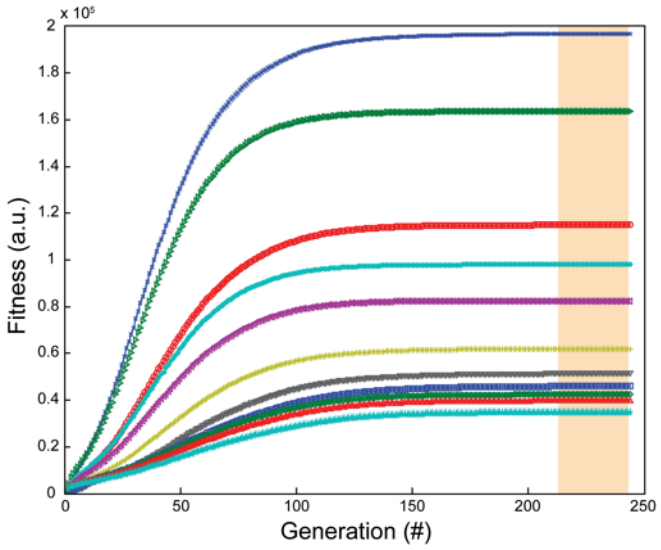

Figure S5: LEA fitness parameter as a function of generation number.

~90 % optimal condition. For all evolutionary algorithms, whether the solution has converged to the globally optimized solution or if it has been caught in a local extrema is impossible to test.[2] Therefore, to determine if the LEA was consistently giving the optimal solution we ran 1,200 simulations at 12 different focal distances between 3 and 14 μm (**Fig. S5**).

Confocal Measurements and Comparison to Simulation for Single Point

A confocal scanning optical microscope (WITec alpha-300) was used to map the 3D optical fields generated from plane-wave light incident on the lattice opto-materials. A fiber-coupled super continuum laser (Koheras SuperK Power Plus) with an acousto-optic tunable filter (AOTF, Koheras Spectrack Dual NIR + 4xVIS) was used to generate collimated (~2 mm beam diameter), unpolarized light at specific operating wavelengths ($\lambda = 690 \pm 2$ or 770 ± 4 nm). For lattices that were measured in air (Figs. 2-4), a 100× air objective (Nikon Plan Fluor, $NA = 0.90$) was used; for lattices measured in high refractive index oil (Fig. 5), a 100× oil objective (Nikon Plan Fluor, $NA = 1.30$) was used. All data was processed using MATLAB©.

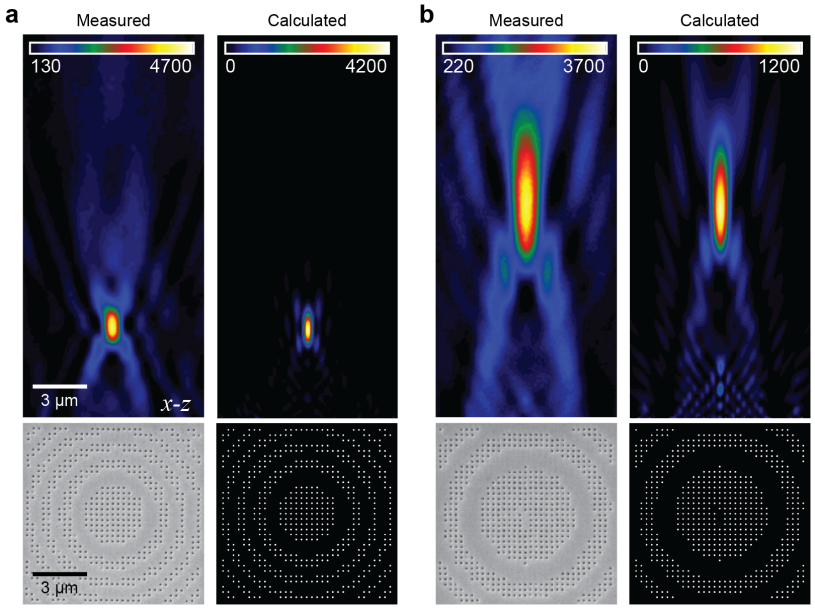

Figure S6: Measured data matches simulated results for lattice opto-materials with a single focal point. SEM images of the lattice structures (lower left) and identical simulated structure (lower right) for (**a**) $f_d = 4$ μm and (**b**) $f_d = 10$ μm. Confocal microscopy field data (upper left, $\lambda = 690$ nm) has the same profile as the corresponding data simulated using the point-source approximation (upper right) for both (**a**) $f_d = 4$ μm and (**b**) $f_d = 10$ μm.

Focal Distances

Using the LEA, we could place a single focal point in any location in the 3D space above the lattice. **Figure S7** shows that a single focal point that is centered along the optical axis could be shifted from 3 μm to 14 μm away from the lattice plane. For refractive microlenses, the focal distance is typically < 0.5 times the lens diameter.[5] Thus, our lattice opto-materials could control light at distances greater than refractive microlenses. As expected, as the focal distance was increased focal point size increased and the intensity decreased.

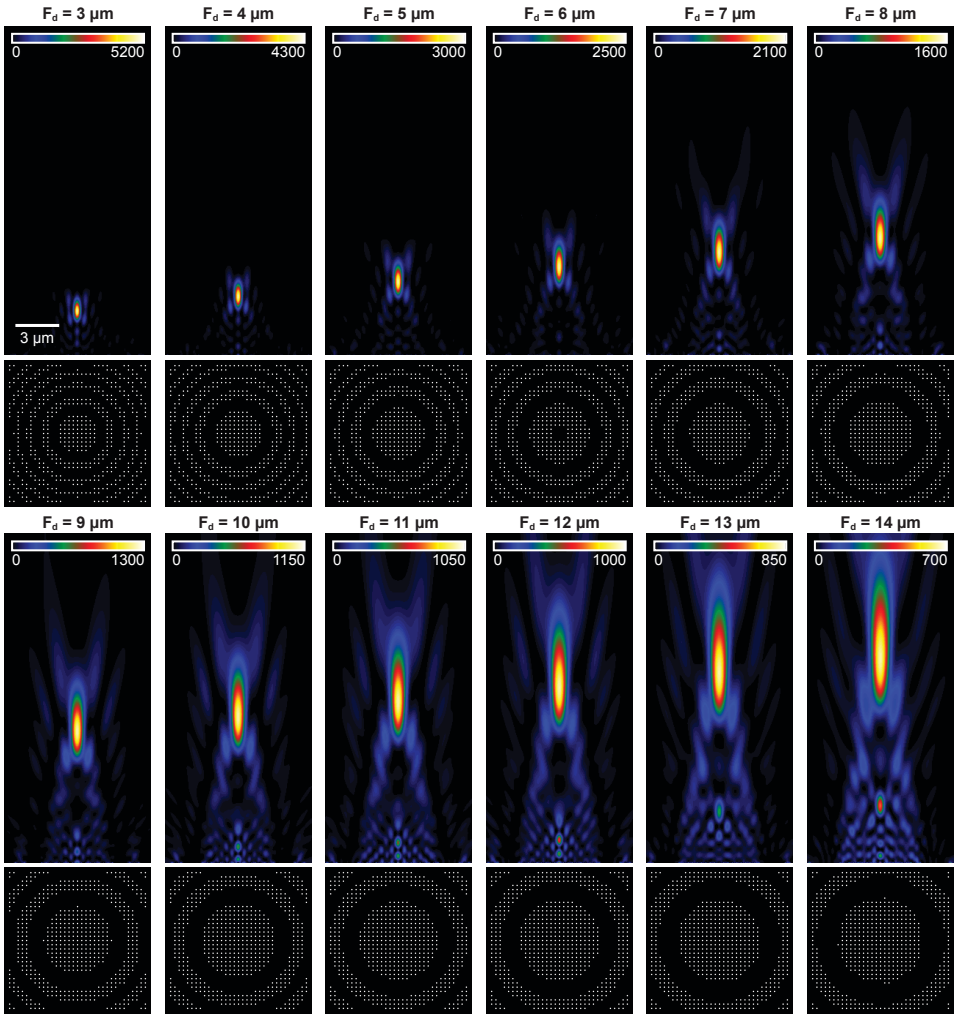

Figure S7: Different focal distances designed by the LEA. By changing the arrangement of nanoholes, we could shift the focal point from 3 μm to 14 μm away from the lattice plane. The focal point was for all 15 lattice opto-materials was within 50 nm of the designed focal point.

Optimization of Parameters for the Lattice Evolution Algorithm

All of the parameters of the LEA including the mutation rate, population size, chromosome length, percent population that has random DNA, and convergence condition must be optimized such that: (i) the LEA gives the best possible configuration of holes for a specified focal distance and (ii) the running time of the LEA is as small as possible. These two optimization conditions are in opposition. For example, decreasing the population size will decrease the simulation time. However, if the population size is too small, the LEA will never find the optimal solution; instead the convergence condition will be met when the LEA is trapped in a local maxima. Increasing the population size, however, will increase the computation time.

To find the optimal parameters for the LEA we tested many different combinations of parameters for the LEA to increase performance. The parameters that resulted in the optimal LEA performance are summarized in **Table S1**. Using these parameters, we found that the focal

Table S1: Optimized LEA parameters

Parameter	Optimal value
Mutation rate	0.001
Population size	600
Chromosome length	3
% with random DNA	12.5
Convergence condition	30 generations

point for all 1200 simulations within ±50 nm of the designed value, which the resolution of the point source simulation. We also found that the standard deviation of the percent change from the maximum intensity was ±0.48% across 1200 simulations with no single simulation with a deviation greater than ±2.00 %.

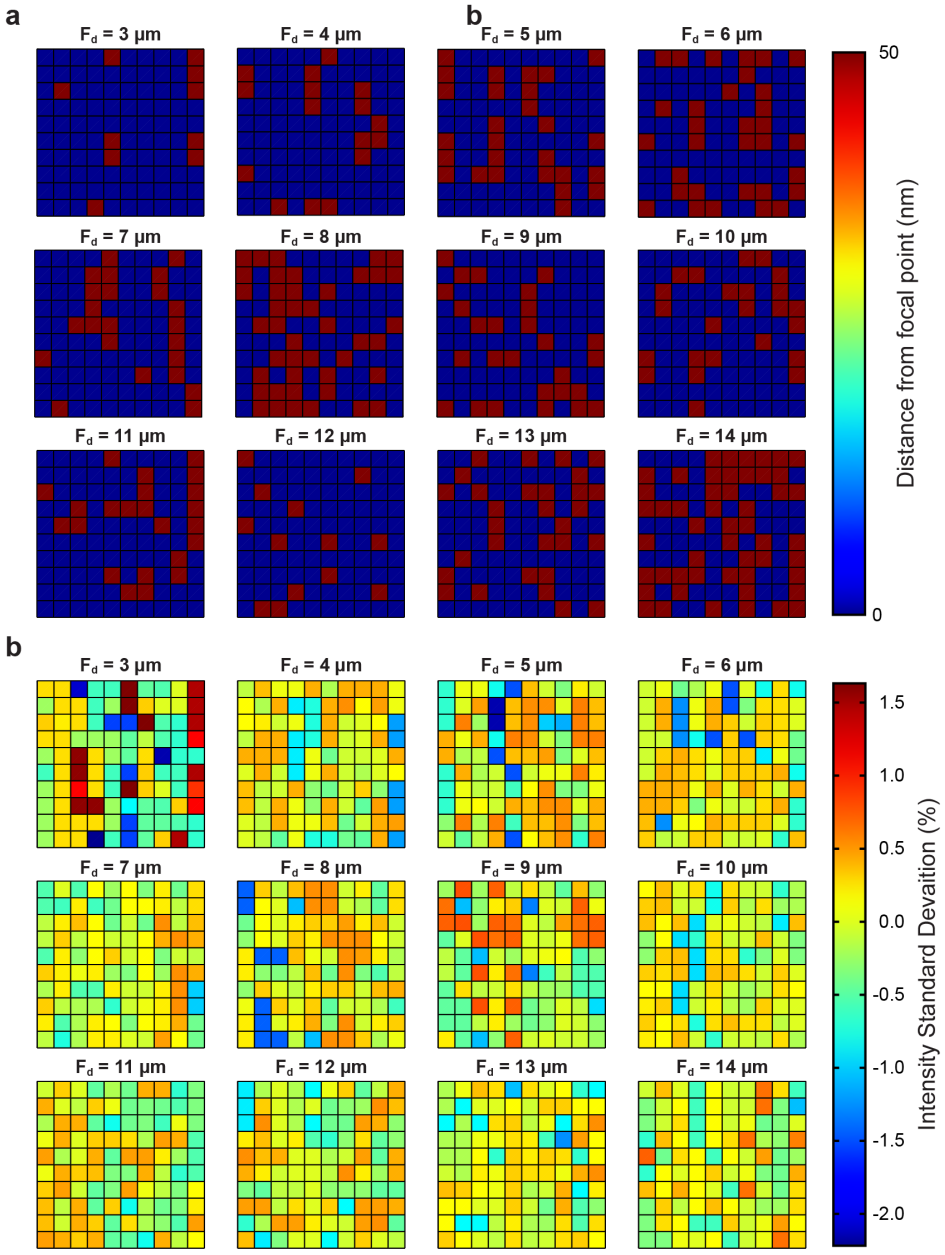

Figure S8: LEA performance 1,200 simulations at 12 different focal distances between 3 and 14 µm. (**a**) For all 1200 simulations were within 50 nm (the resolution of the point source simulation) of the designed value. (**b**) The standard deviation of the percent change from the maximum intensity was ±0.48% across 1200 simulations with no single simulation had a deviation greater than ±2.00 %.

Focused Ion Beam (FIB) Fabrication of Lattice Opto-materials

The pattern of circular or elliptical nanoholes for a specific lattice opto-material was prepared by focused ion beam (FIB) milling (FEI Helios Nanolab) of a 180-nm thick gold film on a glass substrate. Each hole was ~150 nm in diameter and fabricated using a spiral pattern of ion-beam exposures. The number of exposures was used to tune the milling depth while the exposure time was held constant (5 ms). We fabricated lattice opto-materials by drilling holes in a 180-nm thick Au film at locations prescribed by the LEA. Each hole was composed of many exposures with the gallium ion beam. **Figure S7** shows a scheme, which shows the beam pattern for each type of nanohole. In all cases, the beam started in the middle of the hole and proceeded outward. Each exposure point was separated by ~20 nm approximately half of the full-width-at-half-max of the FIB. The gray areas indicate the approximate shape of the hole after exposure (**Fig. S7**).

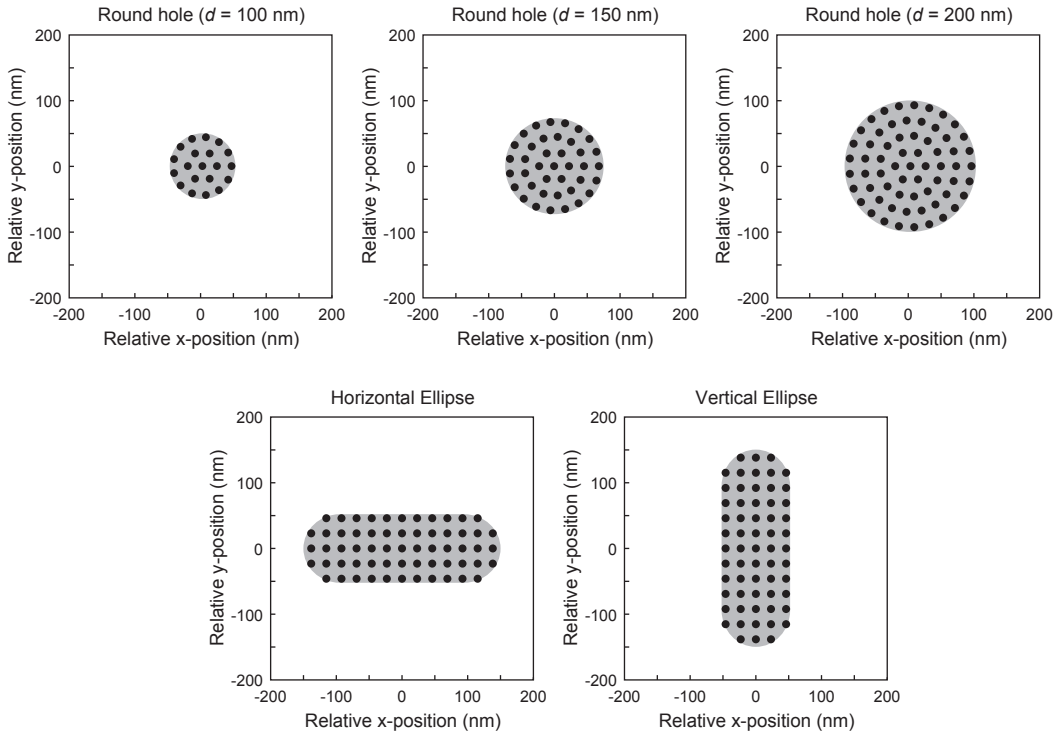

Figure S9: FIB exposure pattern for circular hole with different diameters and elliptical nanoholes.

Script 1: Create FIB pattern from LEA output.

```
%create directory to save the FIB pattern
savePath = 'patterns/';
mkdir(savePath);

%load data from genetic algorithm
fileName='nameOfFileFromGA.dat';
load(fileName);
points = finalData1;

%calibration parameters
t=5; %exposure time in ms
cal = 3.9062e-10*1000000000; %size of a single pixel in nm calibrated with FIB

%set up parameters for a single hole
space = 20; %space between exposure points in nm
buff = space/2; %buffer on the outside of the hole
r=1:(round((75-buff)/space)+1); %radii for all exposure points in a single hole
r=(r-1).*(space/cal);
angle=round((2*pi.*r)./(space/cal)); %angles for all exposure points in a single hole
angle(1)=1;

%write the pattern (locations and exposure time) for a single hole to matrix called "hole"
kk=0;
for ii=1:length(r)
    theta=1:angle(ii);
    theta=theta.*((2*pi)/angle(ii));
    for jj=1:length(theta)
        kk=kk+1;
        hole(kk,1)=t;
        hole(kk,2)=r(ii).*cos(theta(jj));
        hole(kk,3)=r(ii).*sin(theta(jj));
    end
end

%set up parameters for finite array
a0=300/cal; %spacing between lattice points in the array
N=length(points);
width = 10000/cal; %total width of the lattice lens in nm
k=0;
holder=k*length(hole)+1;

%for each lattice point add a hole if prescribed by the genetic algorithm pattern
for i=1:N
    for j = 1:N
        x=i*a0-width/2;
        y=j*a0-width/2;
        if points(i,j)
            pos(holder:holder-1+length(hole),1)=t;
            pos(holder:holder-1+length(hole),2)=hole(:,2)+x;
            pos(holder:holder-1+length(hole),3)=hole(:,3)+y;
            k=k+1;
            holder=k*length(hole)+1;
        end
    end
end

%shift pattern to the center of the FIB area
pos(:,2)=pos(:,2)+(2^16/2);
pos(:,3)=pos(:,3)+(2^16/2);
pos=round(pos); %FIB cannot handle fractional points

%write pattern to a stream file (.str) which can be read by the FIB
dlmwrite([savePath,fileName(1:length(fileName)-4),'.str'],pos,'\t');
```

Each lattice opto-material was composed of hundreds of the nanohole patterns according the pattern given by the LEA. Therefore we wrote a script that converted the output of the LEA into a pattern file, called a stream file that could be read by the FIB control software (**Script 1**). The

stream file contains the *x* and *y* coordinates as well as the exposure time for every exposure point in the pattern. A typical stream file contained ~25000 points. During patterning, all of the points in the stream pattern were looped over until the FIB milled completely through the 180-nm thick Au film. To tune the depth of the FIB milling, we chose to keep the exposure time constant (5 ms) and adjusted the number of times that the pattern file was iterated over. A typical number of iterations was ~1100; however, since the conditions of the FIB changed from session to session, we always tested this number before creating lattice opto-materials. Typically a single lattice opto-material pattern could be made in ~2 min. Since we were interested in making many different lattice opto-materials on the same Au film, we wrote a script using the AutoFIB© scripting software to move the stage and create different patterns that were separated by 100 μm in the *x*- and *y*-directions.

Lattice Opto-materials with the Same Focal Distance for Different Wavelengths

Lattice opto-materials could be designed with any wavelength to focus light to any location along the optical axis. Confocal measurements matched the simulated results. As expected, the focal points of the smaller wavelength samples were smaller and followed the diffraction limit (**Fig. S6**). In future work, we could use the LEA to design lattice opto-materials without chromatic aberration.

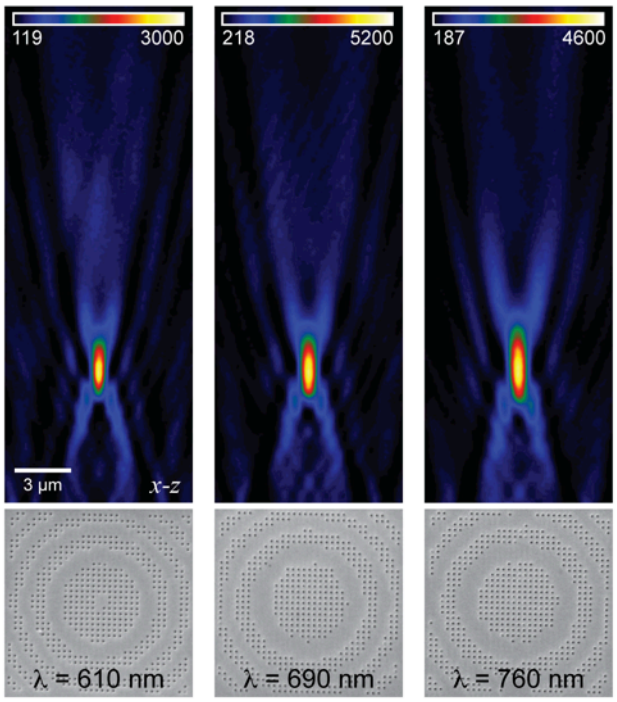

Figure S10: Lattice evolutionary algorithm solutions at different wavelength but the same focal distance f_d = 7 μm. Three lattice opto-materials designed at λ = 610, 690 and 780 nm respectively (left to right).

Lattice Evolution Algorithm for Multiple Focal Points

The normalization of each individual fitness functions is necessary so that LEA will optimize for both focal points equally even if one of the focal points has a higher maximum intensity. Since the fitness functions were normalized to their own maximum at every generation, the maximum of the total fitness function will change with every generation. Therefore, to check for

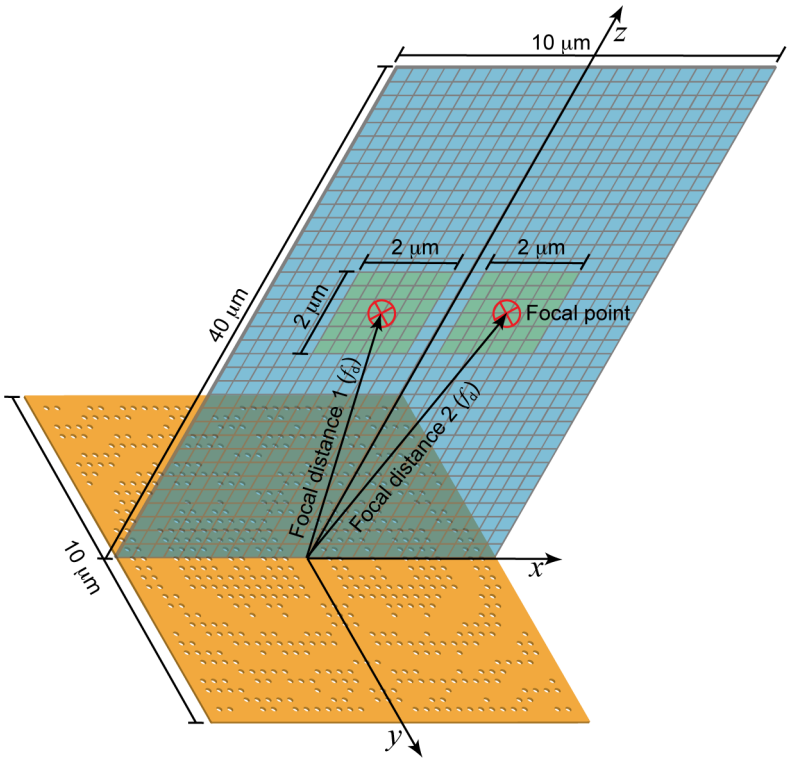

Figure S11: Schematic calculation window for the LEA with two focal points. The two windows where the field was calculated for the LEA are shown in green.

the convergence condition, we used the sum of the fitness function for each location without normalizing. Increasing the number of focal points, however, significantly increased the convergence time from ~0.45 cpu hours for a single focal point to ~96 cpu hours for seven. The reason is that the numbers of field points that need to be calculated increase linearly with the number of focal points. Additionally, for multi-objective problems, there are more local maxima and minima, which increases the time required for convergence.

Comparison of Simulated and Measured Data for Two Focal Points

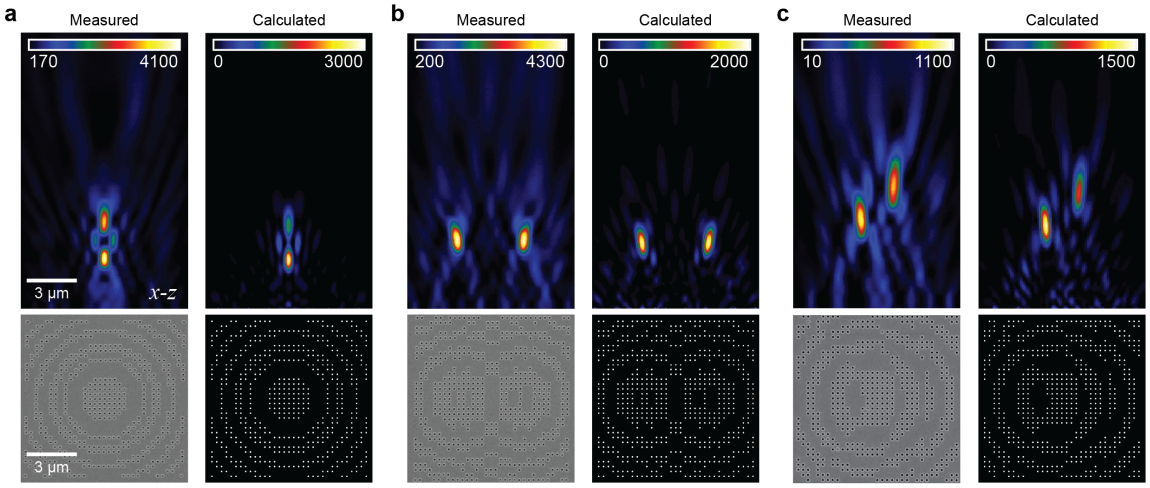

Figure S12: Measured data matches simulated results for lattice opto-materials with two focal points. SEM images of the lattice structures (lower left) and identical simulated structure (lower right) for all lattice opto-materials. Confocal microscopy field data (upper left, $\lambda = 690$ nm) has the same profile as the corresponding data simulated using the point-source approximation (upper right) for all lattice opto-materials. The lattice plane as $z = f_d = 0$ and the center as $x = 0$. The two focal points were located at (**a**) $f_d = 4$ μm, $x = \pm 2$ μm, $y = 0$; (**b**) $f_d = 3, 5$ μm, $x = 0$, $y = 0$; and (**c**) $f_d = 5, 7$ μm, $x = \pm 1$ μm, $y = 0$

Comparison of Simulated and Measured Data for 3, 5 and 7 Focal Points

Figure S13 shows measured *x*-*y* cross sections for lattice opto-materials that were designed to concentrate light at 3, 5 and 7 locations. We tested prime numbers to illustrate that these solutions were not a result of diffraction from the Talbot effect. Since the fitness function is designed to optimize the intensity at the desired focal points, other locations of high intensity may unintentionally emerge. For example, **Fig. 3c** shows a high intensity spot located along the optical axis and below the focal plane, which is also seen in simulation. A more complicated fitness function, however, could eliminate these types of artifacts.

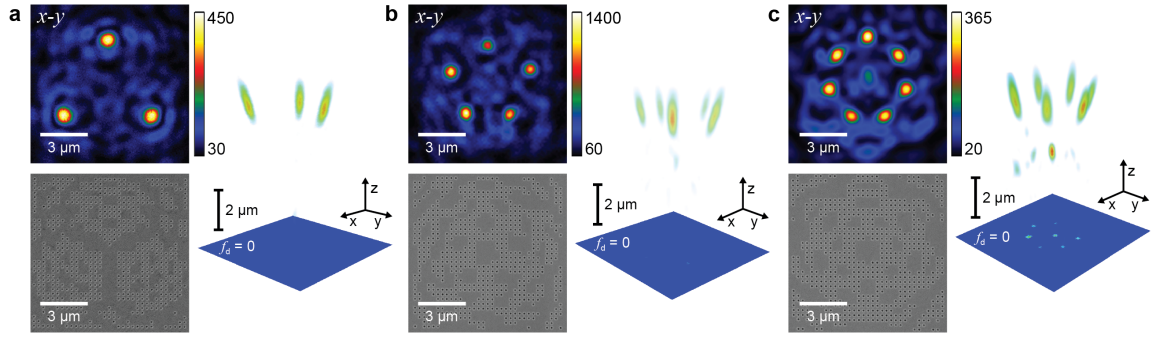

Figure S13: Lattice opto-materials can generate arbitrary light profiles in 3D. SEM images of the lattice structures (lower), 2D confocal microscopy slices at f_d = 7 µm (upper, λ = 690 nm), and 3D volume pattern (right). All focal points had a constant distance (r) from the center of the lattice and were evenly spaced around the center. (**a**) Three focal points at f_d = 7 µm and r = 3 µm. (**b**) Five focal points at f_d = 7 µm and r = 2.5 µm. (**c**) Seven focal points at f_d = 7 µm and r = 2.5 µm.

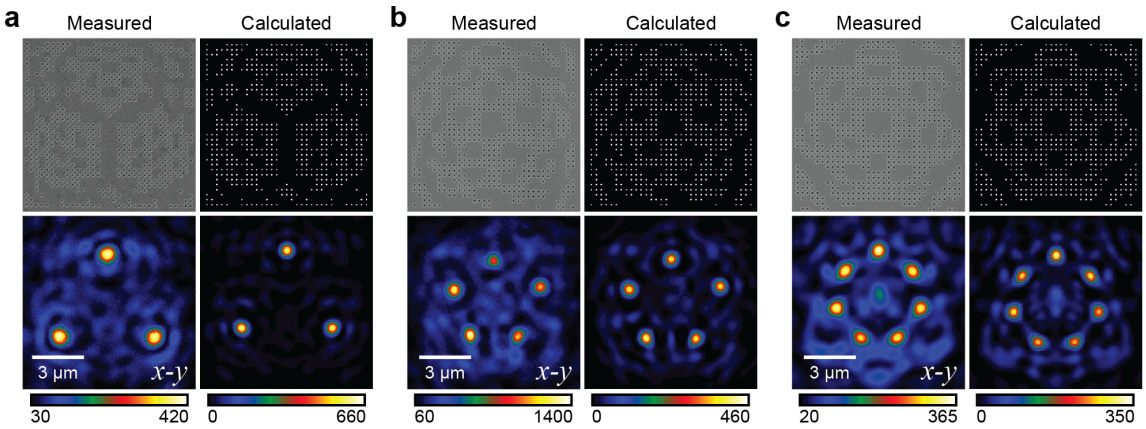

Figure S14: Measured data matches simulated results for lattice opto-materials with 3, 5, and 7 focal points. SEM images of the lattice structures (upper left) and identical simulated structure (upper right) for all lattice opto-materials. Confocal microscopy field data *x*-*y* cross section (lower left, λ = 690 nm) has the same profile as the corresponding data simulated using the point-source approximation (upper right) for all lattice opto-materials. All focal points had a constant distance (*r*) from the center of the lattice and were evenly spaced around the center. (**a**) Three focal points at f_d = 7 μm and *r* = 3 μm. (**b**) Five focal points at f_d = 7 μm and *r* = 2.5 μm. (**c**) Seven focal points at f_d = 7 μm and *r* = 2.5 μm.

Lattice Opto-materials with Multiple Phase Elements

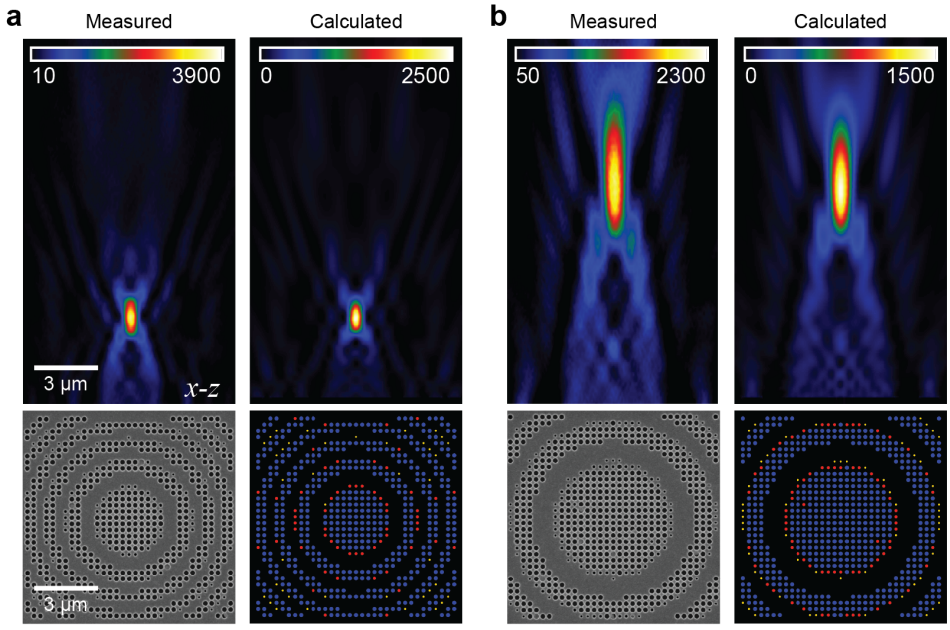

Figure S15: Measured data matches simulated results for lattice opto-materials with multiple phase elements. Scanning electron microscope (SEM) images of the lattice structures (lower left) and identical simulated structure (lower right) for (**a**) f_d = 4 μm and (**b**) f_d = 10 μm. The different hole sizes are represented by blue, d = 200 nm; red, d = 150 nm; and yellow, d = 100 nm. Confocal microscopy field data (upper left, λ = 690 nm) has the same profile as the corresponding data simulated using the FDTD simulation (upper right) for both (**a**) f_d = 4 μm and (**b**) f_d = 10 μm.

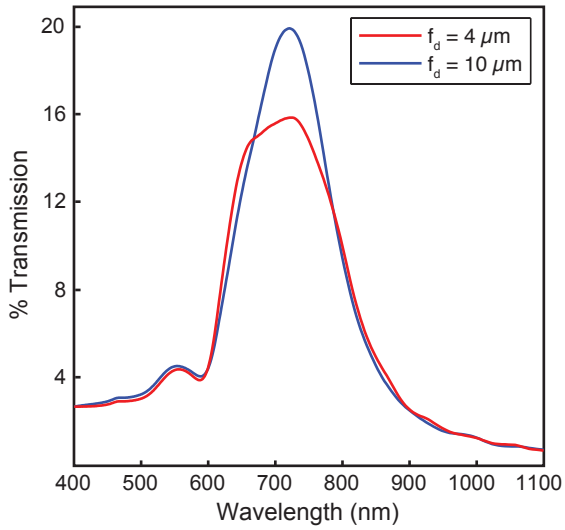

Figure S16: Far-field optical spectra for lattices with multiple phase elements calculated by FDTD methods. The calculated transmission efficiency was near 20%.

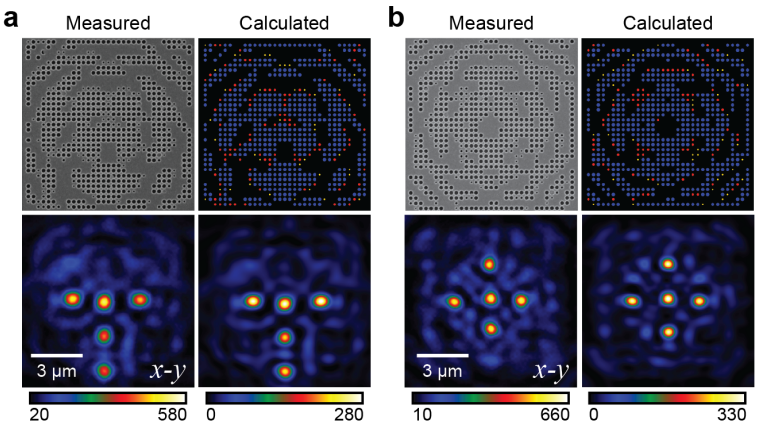

Figure S17: Measured data matches simulated results for lattice opto-materials with 3 phase elements. SEM images of the lattice structures (upper left) and identical simulated structure (upper right) for all lattice opto-materials. The different hole sizes are represented by blue, d = 200 nm; red, d = 150 nm; and yellow, d = 100 nm. Confocal microscopy field data x-y cross section (lower left, λ = 690 nm) has the same profile as the corresponding data simulated using the FDTD simulations (upper right) for all lattice opto-materials. (**a**) Five focal points at f_d = 7 μm in a "T" shape with 1 μm separation between points. (**b**) Five focal points at f_d = 5 μm in an "X" shape with 1 μm separation between points.

Transmission Spectra for Gold Lattice Opto-materials

To find the peak in the transmission spectra, we simulated finite arrays of nanoholes with a 300-nm periodicity. To ensure that the different lattice opto-material configurations did not affect the far-field spectra, we tested lattices with different focal distances. **Figure S18** shows that all of the lattice opto-materials that had round holes had a transmission peak ~ 690 nm. For the elliptical holes, the transmission peak red-shifted by ~80 nm. Thus, the polarization-dependent lattice opto-materials were designed and measured at λ = 770 nm. Since the peak in transmission is caused by extraordinary optical transmission (EOT), which is mediated by surface plasmon polaritons, the location of the peak can be blue- or red-shifted by increasing or decreasing the periodicity of the holes in the arrays.

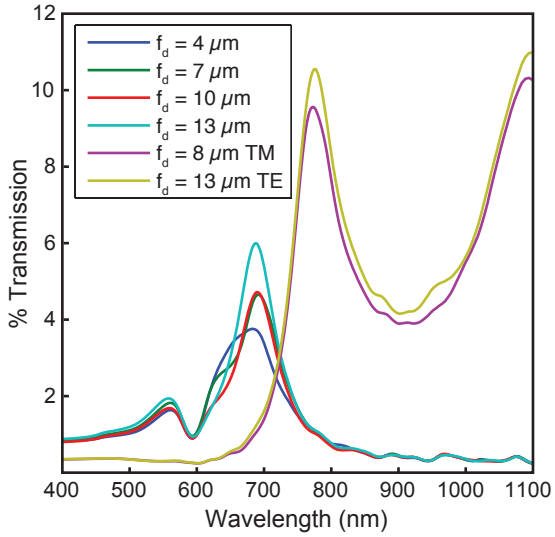

Figure S18: Far-field optical spectra for lattices with round and elliptical holes calculated by FDTD methods. Changing the hole shape from round to elliptical red-shifts the transmission peak from 690 nm to 770 nm.

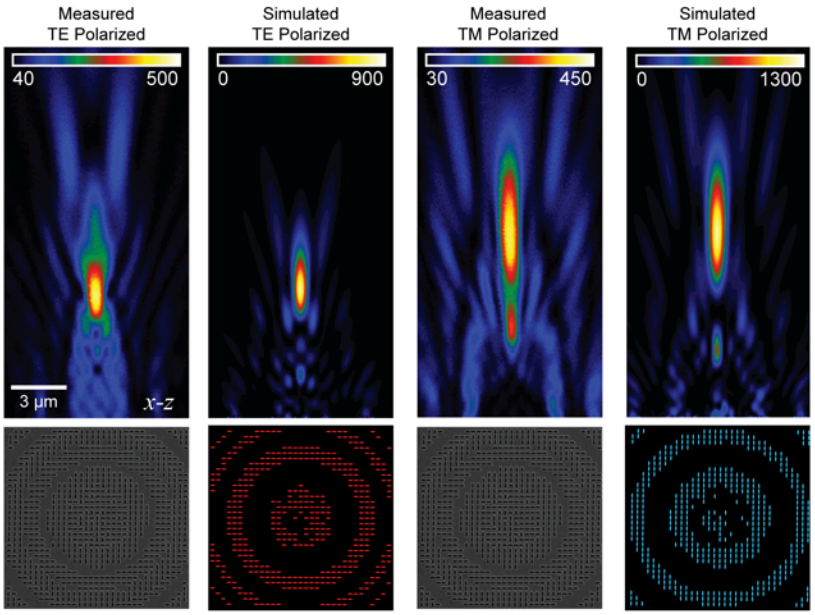

Figure S19: Polarization dependent focal point. TE polarized light focuses light at f_d = 7 μm and TM polarized light focuses light at f_d = 10 μm. The measured confocal microscopy field data (λ = 770 nm, **left**) match well with the simulated results (**right**).

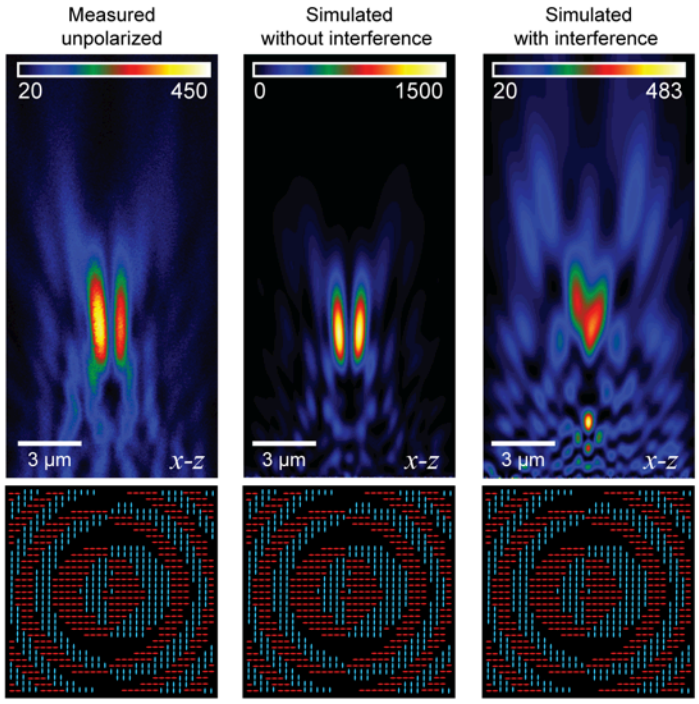

Figure S20: Comparison of confocal microscopy field data (λ = 770 nm) with unpolarized light to simulation data both with and without interference effects.

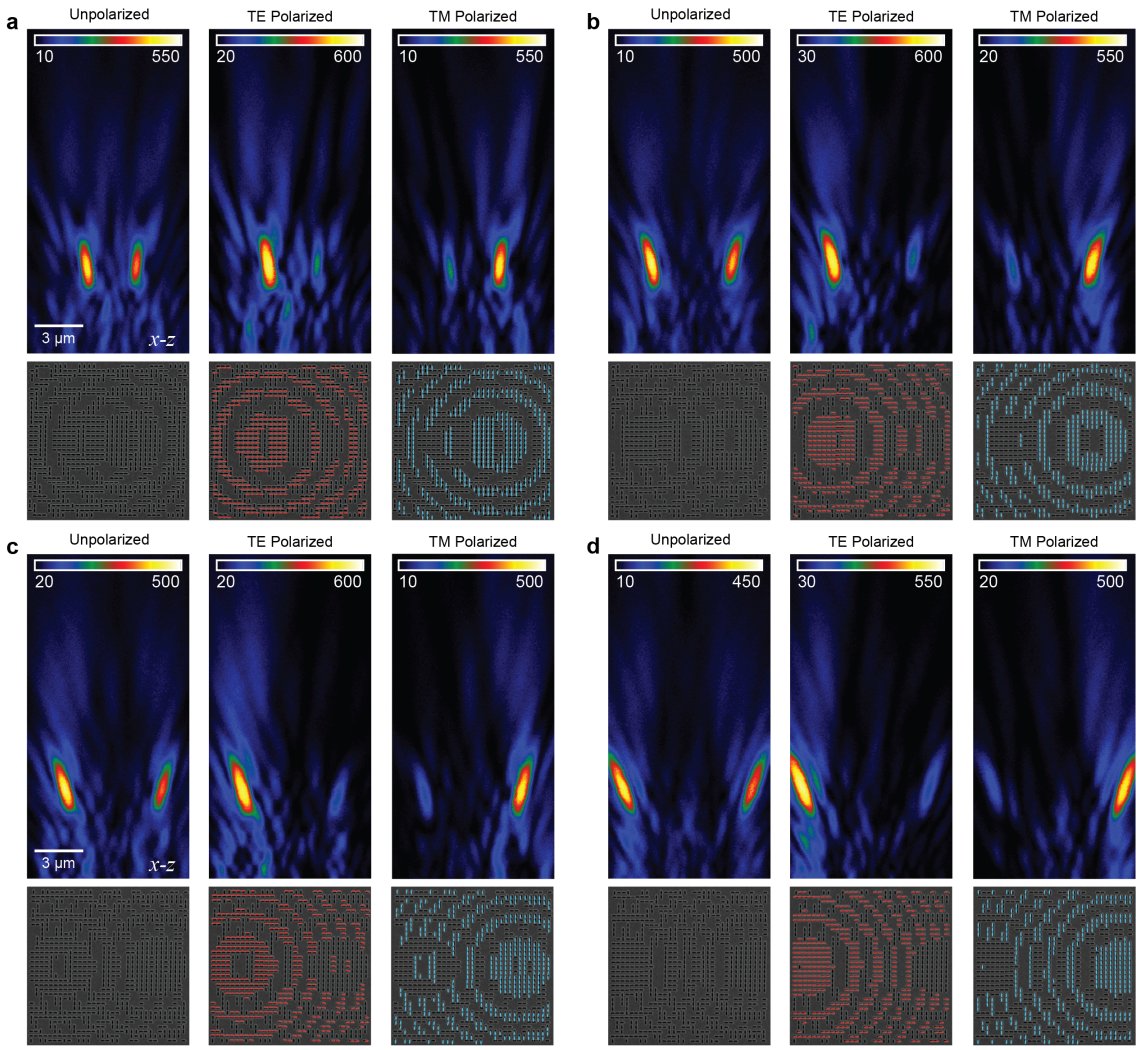

Figure S21: Polarization dependent focal point. SEM images (lower) and confocal microscopy field data (λ = 770 nm, upper) of polarization-sensitive lattice opt-materials. The polarization-sensitive lattice opt-materials were measure with unpolarized, TE and TM polarized light. The holes that were active under TE and TM polarization are highlighted in red and blue respectively. Polarization-sensitive lattice opt-materials with dynamic focal shift (Δx) that focus light at f_d = 5 μm and shifted by 3 μm (**a**), 5 μm (**b**), 6 μm (**c**), and 8 μm (**d**).

Bright-field and Confocal Measurements of Compound Lattice Optics

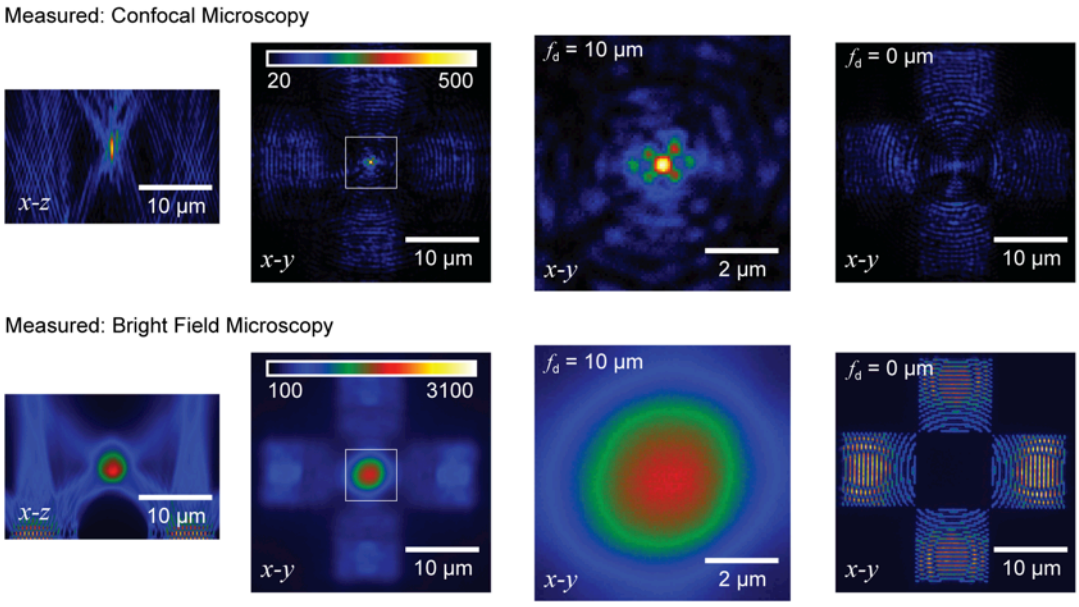

Figure S22: Comparison of confocal and bright field microscopy measurements of 2D compound optics for imaging applications. (**upper**) Confocal microscopy data (λ = 690 nm) 2D *x-y* cross-sections of the four interfering lattice opt-materials at the height of the focal distance (f_d = 10 µm) and an *x-z* cross-section across the center of the lattice. (**lower**) Bright field microscopy data (λ = 700±40 nm) 2D *x-y* cross-sections of the four interfering lattice opt-materials at the height of the focal distance (f_d = 10 µm) and an *x-z* cross-section across the center of the lattice. Bright field measurements were taken with a 100× oil objective (Nikon Apo TIRF, *NA* = 1.49).

Supporting References

1. Goldberg, D. E. *Search, Optimization and Machine Learning* **1989**, 343-349.
2. Davis, L. *Handbook of Genetic Algorithms*; Van Nostrand Reinhold: New York, 1991.
3. Doucet, A.; De Freitas, N.; Gordon, N. *Sequential Monte Carlo Methods in Practice*; Springer: New York, New York, 2001.
4. Gao, H.; Hyun, J. K.; Lee, M. H.; Yang, J.-C.; Lauhon, L. J. Odom, T. W. *Nano Lett.* **2010**, *10*, 4111−4116.
5. Popovic, Z. D.; Sprague, R. A.; Connell, G. A. N. *Appl. Opt.* **1988**, *27*, 1281−1284.